Applied Catalysis B: Environmental 331 (2023) 122664

Contents lists available at ScienceDirect

Applied Catalysis B: Environmental

journal homepage: www.elsevier.com/locate/apcatb

Hydrogen anode/cathode co-productions-coupled anode alcohol selective oxidation and distinctive H/e transfer pathways

Di Si [a], Min Wang [b], Xue Yang [c], Cheng Wang [c], Kai Shi [a], Bingji Huang [a], Lisong Chen [a,d,*], Jianlin Shi [b,**]

[a] Shanghai Key Laboratory of Green Chemistry and Chemical Processes, School of Chemistry and Molecular Engineering, East China Normal University, Shanghai 200062, PR China
[b] State Key Laboratory of High Performance Ceramics and Superfine Microstructures, Shanghai Institute of Ceramics, Chinese Academy of Sciences, Shanghai 200050, PR China
[c] Sinopec Research Institute of Petroleum Processing, Beijing 100083, PR China
[d] Institute of Eco-Chongming, Shanghai 202162, PR China

ARTICLE INFO

Keywords:
Alcohol-oxidation
Co-production
HER
Electrocatalysts

ABSTRACT

Co-electrolysis, which can produce more than one kind of high value products concurrently at lowered energy cost, has attracted increasing attention. However, the development of novel co-electrolysis systems and efficient electro-catalysts, and the investigation of corresponding reaction mechanism, are urgently needed. Anodic biomass oxidation-coupled electrocatalytic anode/cathode hydrogen co-production has been attracting intense attentions most recently. Herein, a co-electrolysis system of α-H-armed alcohols and water has been established by introducing an efficient PdBi/NF electrocatalyst, in which hydrogen can be obtained from both anode and cathode, and alcohols can be selectively oxidized to corresponding high-value chemicals. In particular, valuable 3-Hydroxypropionic acid (3-Hp) at the anode, together with hydrogen gas at both cathode and anode, can be obtained by the co-electrolysis of water and 1, 3-propanediol (1, 3-P). More importantly, the reaction mechanism, especially the hydrogen atom and electron transfer pathway have been investigated in detail, which has been overlooked in previous literatures.

1. Introduction

The increasing global energy demand and critical concern of climate change resulting from fossil fuel burning have triggered considerable efforts in developing sustainable and clean energy storage and conversion technologies. Electrolysis uses electricity generated from renewable energy sources, such as solar, wind and hydraulic energy to produce high value-added chemical products, providing a highly promising technique for a sustainable society. Nowadays, electrocatalytic water splitting for hydrogen evolution reaction (HER) has become hot topics on the frontiers of clean energy science and technology [1–5].

Conventional electrocatalytic systems usually focus on obtaining a single-target chemical (Fig. 1a) [6a], in which, however, serious side and competitive reactions must be suppressed and the high energy barrier of counterpart reactions must be lowered to industrialize such electrocatalytic systems. Therefore, novel electrocatalytic systems, especially co-electrocatalysis, have been designed to electrolyze more than one kind of chemical precursors at the same time for the productions of multiple high value-added products at favorably lowered energy input [6b]. Kinetically favorable reactions will take place much more easily, i.e., at much higher rates, than the kinetically less-favorable reactions once two or multiple precursors are added to one cell, therefore resulting in lowered energy consumption (Fig. 1b) [6c]. Alcohol ($R–CH_2OH$) electrooxidation has been used to accelerate hydrogen production from water splitting, in which, unfortunately, the eliminated hydrogen atom(s) deprived from C–H bond(s) of the alcohol molecules will be oxidized into H_2O by the Volmer step ($*H + OH^- \rightleftharpoons * + H_2O + e^-$), leading to unsatisfactory atom-efficiency in the conventional alcohol electrooxidations [6d]. Recently, low-potential aldehyde oxidation combined with water splitting for simultaneous hydrogen

* Corresponding author at: Shanghai Key Laboratory of Green Chemistry and Chemical Processes, School of Chemistry and Molecular Engineering, East China Normal University, Shanghai 200062, PR China.
** Corresponding author.
E-mail addresses: lschen@chem.ecnu.edu.cn (L. Chen), jlshi@mail.sic.ac.cn (J. Shi).

https://doi.org/10.1016/j.apcatb.2023.122664
Received 11 December 2022; Received in revised form 17 March 2023; Accepted 18 March 2023
Available online 24 March 2023

evolution at anode and cathode has been firstly established by Wang et. al.[7a], which demonstrates the feasibility of bipolar hydrogen featuring single gas production and satisfactory atom-efficiency. Therefore, it is of great significance to further develop co-electrolysis systems to produce hydrogen from both anode and cathode at elevated productivity, and additional value-added chemicals. Despite its great promises for applications, most of the attention was focused on aldehydes [7b]. Moreover, abundant alcohols, instead of high value aldehyde, should be more promising precursors for the anode oxidation to produce value-added chemicals.

$$R-CH_2OH+2OH^-\rightarrow RCOO^-+H_2O+xH_2+ye^- \quad (1)$$

$$2H_2O+2e^-\rightarrow H_2+2OH^- \quad (2)$$

Herein, a co-electrolysis system of water and alcohol has been established for the efficient anodic production of value-added oxidative carboxylic acid product, and the concurrent hydrogen evolutions from both anode and cathode (Fig. 1c, Reaction 1–2), in which 1, 3-propanediol (1, 3-P) has been firstly chosen as the model alcohol in this system. It is known that four α-H atoms-armed 1, 3-P produced from glucose or glycerol is a low-cost and renewable resource, and its world market volume in 2013 amounted to 140 kilotons [8]. Meanwhile, 3-Hydroxypropionic acid (3-Hp), a desired product of 1, 3-P oxidation, ranks third in the synthetic raw materials of biological resources [9–12], suffers greatly from poor selectivity and heavy energy cost in the chemical and biological productions (Fig. S1a-b) [13–15]. Therefore, the electrocatalytic synthesis of 3-Hp by 1, 3-P oxidation is thought to be highly attractive and industrially promising, surprisingly, however, no related report can be found so far.

A Pd-based electrocatalyst, dendritic PdBi grown on Ni foam (PdBi/NF) has been developed as an efficient anodic electrocatalyst (Fig. S1c) to produce 3-Hp and hydrogen by taking advantage of α-H and electrons from alcohols. Furthermore, the detailed reaction mechanism for the co-electrolysis system, especially the hydrogen and electron reaction pathways, has been probed in-depth. The experimental and computational results demonstrate that a fraction of hydrogen atoms and electrons from the oxidation of the 1, 3-P are used distinctively for anode hydrogen production and catalyst activation without entering the circuit. Simultaneously, the remaining electrons are transferred through the circuit to the cathode for HER (3.21 mL cm^{-2} h^{-1}). Such a co-electrolysis strategy has been extended to the anodic oxidations of a number of alcohols for the co-productions of hydrogen from both anode and cathode, and highly valuable chemicals.

2. Experimental section

2.1. Chemicals

Sodium tetrachloropalladate (Na_2PdCl_4, 34% Pd), Bismuth trichloride ($BiCl_3$, 98%), and Sulfuric acid (H_2SO_4, 99.5%), ethanol (EtOH, 99.9%) hydrochloric acid (HCl, 37.0%), 1, 3-Propanediol ($C_3H_8O_2$, 99.0%), 3-Hydroxypropionic acid ($C_3H_6O_3$, 99.0%), 1, 4-Butanediol ($C_4H_{10}O_2$, 99.0%), 1, 5-Pentanediol ($C_5H_{12}O_2$, 99.0%), Propylene glycol ($C_3H_8O_2$, 99.0%), Isopropyl alcohol (C_3H_8O, 99.0%), 1-Propanol (C_3H_8O, 99.0%), Glycerol ($C_3H_8O_3$, 99.0%), Phthalic acid ($C_8H_6O_4$, 99.0%), Maleic acid ($C_4H_4O_4$, 99.0%), Heavy-oxygen water ($H_2^{18}O$), Deuterated water (D_2O) were purchased from Adamas Reagent Co., Ltd. Potassium carbonate (K_2CO_3, 90.0%), Potassium hydroxide (KOH, 90.0%) were from Macklin. All chemicals were used as received without any further purification. Deionized water (DIW) was used in all experiments.

2.2. Preparation of PdBi/NF

Before electrodeposition, the nickel foam (NF) was cut into small pieces (2 ×2 cm), followed by sequentially washing with HCl, deionized water, and ethanol. The electrodeposition was performed in a three-electrode system, using saturated calomel electrode (SCE) and a platinum foil as reference and counter electrodes respectively. Typically, the PdBi/NF was prepared in an aqueous solution with 3.6 mM noble metal precursors (Na_2PdCl_4), 0.8 mM $BiCl_3$ and 0.5 M H_2SO_4 by applying a constant potential of − 0.3 V vs SCE for 800 s. The final product was washed several times by deionized water. Finally, the as-prepared PdBi/NF was dried in an oven at 60 ℃. The synthesis of Pd/NF, Bi/NF were similar to that of PdBi/NF, except that $BiCl_3$, Na_2PdCl_4 were selectively added. PdBi/NF-1, PdBi/NF-2, PdBi/NF-3, PdBi/NF-4, PdBi/NF-5 were electrodeposited on the NF substrate using a three-electrode cell as described above at a constant potential of different time, − 0.3 V for 100 s, 300 s, − 0.1 V for 800 s, 300 s and − 0.3 V for 1200 s, respectively.

2.3. Characterizations of nanostructure

X ray diffraction pattern (XRD) spectra were performed on a Rigaku D/MAX 2550 diffractometer with Cu Ka radiation (l = 1.5418 Å). Scanning electron microscope (SEM) images were carried out on a Hitachi S-4800 SEM, operating voltage 3 kV. TEM images were carried out on a JEM-2100 F, accelerating voltage 200 kV. The compositions of catalysts were determined by X-ray photoelectron spectroscopy (XPS, Thermo ESCALAB 250Xi) with Mg Kα radiation source (hν = 1253.6 eV). The deconvolution of the Bi, Pd, Ni, C and O was performed through a software CasaXPS.

2.4. Electrochemical measurements

Electrochemical tests for 1, 3-Propanediol oxidation, and oxygen evolution reaction (OER), HER were performed on a BioLogic VSP-300 electrochemical workstation in a typical three-electrode single cell at room temperature with 1 × 1 cm^2 of the as made materials as the working electrode, a Pt plate as the counter electrode and a Hg/HgO

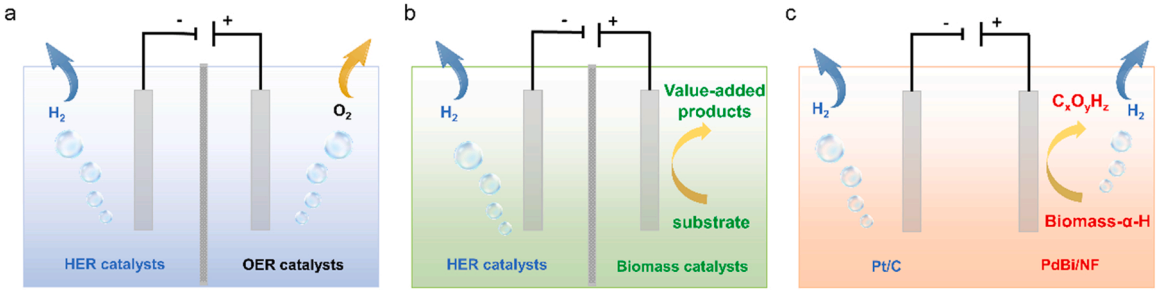

Fig. 1. Design schematics of electrolysis. (a) conventional water electrolysis for HER at the cathode, **(b)** co-electrolysis for cathodic HER and anodic organic molecule oxidation for chemicals, and **(c)** anodic and cathodic hydrogen co-evolutions, in addition to the anodic chemical production, in a proposed water and α-H-armed alcohol co-electrolysis system.

(1.0 M KOH) as the reference electrode, respectively. The hydrogen production measurements were conducted in an H-type electrochemical cell, in which an alkaline polymer electrolyte membrane (Alkymer, w-25) was used for electrode separation. Hg/HgO (1.0 M KOH) reference electrode was calibrated with respect to RHE in high purity hydrogen saturated 1.5 M KOH electrolytes, two platinum wire electrodes were used as the counter electrode and the working electrode in this measurement, respectively. For two electrode test, PdBi/NF was used as anode and platinum plate as cathode. The electrochemical active surface area (ECSA) of the tested catalysts could be investigated by cyclic voltammetry (CV) in an electrolyte of 1.5 M KOH solution containing 1 M 1, 3-Propanediol. Electrochemical impedance spectra (EIS) were carried out in a frequency range from 100 kHz to 0.1 Hz with 5 mV amplitude. The electrochemical double layer capacitances (C_{dl}) of various materials could be investigated by cyclic voltammetry in the potential region where the faradaic process doesn't exist. Linear sweep voltammetry (LSV) were measured at a scan rate of 5 mV s^{-1}. 1, 3-Propanediol oxidation reaction tests were conducted in a 1.5 M KOH solution containing 1 M 1, 3-Propanediol. The area of the working electrode in the electrolyte was fixed at 1×0.7 cm^2 and all current densities were normalized to the geometrical area of the electrode. No IR compensation has been done for all above data.

2.5. Product Quantification

The 1, 3-Propanediol oxidation products were determined and the corresponding Faradaic efficiencies were calculated. Firstly, the electrocatalytic oxidation of 1, 3-Propanediol was conducted at a constant potential for 2 h. Then 500 μL aliquots of the electrolyte were collected and diluted with 200 μL of Dimethyl-d6 sulfoxide which were then analyzed by nuclear magnetic resonance (NMR) spectrometer. Phthalandione was used as internal standard. ^1H and ^{13}C NMR spectra were obtained on an Avance II 300 instruments (Bruker). A Ramin GC2060 gas chromatograph with a packed column and a thermal conductivity detector was used to quantify the generated O_2 and H_2 generated at the cathode and anode during electrolysis. The oven temperature was set at 60 °C, and nitrogen was used as the carrier gas.

Conversion of the organic substrates and FE were calculated on the basis of the following equations:

$$Conversion(\%) = (1 - n[mole]_{aftereletrolysis} \Big/ n[mole]_{beforeeletrolysis}) \times 100$$

$$Faradayefficiency(\%) = (n[mole]_{experimentallyproduced} \Big/ n[mole]_{theoreticallyproduced}) \times 100$$

where n[mole] is the mole number of the substrate. The theoretically produced amount was calculated on the basis of

$$n[mole]_{theoreticallyproduced} = Q \Big/ (n \times F)$$

where Q is the transferred charge, n is the number of electrons transferred for each product molecule and F is Faraday's constant (96,485 C mol^{-1}).

2.6. Isotope Labeling Experiments: 1, 3-Propanediol oxidation over PdBi/NF in alkaline H_2O, $H_2^{18}O$ or D_2O solvent

Initially, 1 M 1, 3-Propanediol dispersed respectively in alkaline H_2O, $H_2^{18}O$ or D_2O solvent (1.5 M KOH) were oxidized over PdBi/NF in the standard conditions for 2 h. The final product (3-Hydroxypropionic acid) were neutralized with sulfuric acid to remove salt and then extracted with ethyl acetate followed by rotary desorption to remove organic reagents for GC/LC-MS analysis. Gas is analyzed by GC.

2.7. Operando Raman spectroscopy measurements

Electrochemical operando Raman measurement was carried out by a Raman spectroscopy (LABRAM HR Evolution, HORIBA) under an excitation of 532 nm laser light and electrochemical workstation. 1.5 M KOH with 1 M 1, 3-P was used as the electrolyte. The Raman spectroscopy was recorded at different potentials and time.

2.8. Electrochemical in situ fourier transform infrared (FTIR) spectroscopy

Electrochemical in situ FTIR measurements were performed on a Linglu instruments ECIR-II cell mounted on a Pike Veemax III ATR with a single bounce silicon crystal covered with a Au membrane in internal reflection mode. Spectra were recorded on a Thermo Nicolet Nexus 670 spectrometer. The electrolyte was degassed by bubbling N_2 for 30 min before the measurement. The single bounce silicon crystal covered with a Au membrane was prepared through the following procedure. (a) The silicon was immersed into 20 mL of aqua regia (V_{HCl} /V_{HNO3} =1:3) and polished using 50 μm alumia. (b) The silicon was washed three times with water and acetone, respectively. (c) The silicon was transferred into a piranha solution (V_{H2SO4}/V_{H2O2} =3:1). (d) The as prepared oxidized silicon was then immersed into NH_4F solution (40%) for 5 min and transferred into the mixture solution of gold plating solution (15 mL) and HF (2%, 3.4 mL) for 5 min. The gold plating solution was prepared through dissolving NaOH (0.12 g), $NaAuCl_4 \cdot 2\,H_2O$ (0.23 g), NH_4Cl (0.13 g), Na_2SO_3 (0.95 g) and $Na_2S_2O_3 \cdot 5\,H_2O$ (0.62 g) in 50 mL water. In a typical procedure for the fabrication of the working electrode, 10 mg catalysts and 25 μL of 0.5% Nafion solution were dispersed in 5 mL deionized water by sonication to generate a homogeneous ink. Then, 0.2 mL of the ink (containing 600 μg catalysts) was transferred onto the gold membrane.

2.9. DFT calculation details

We have employed the Vienna Ab Initio Package (VASP) to perform all the density functional theory (DFT) calculations within the generalized gradient approximation (GGA) using the PBE formulation. We have chosen the projected augmented wave (PAW) potentials to describe the ionic cores and taken valence electrons into account using a plane wave basis set with a kinetic energy cutoff of 520 eV. Partial occupancies of the Kohn−Sham orbitals were allowed using the Gaussian smearing method and a width of 0.05 eV. The electronic energy was considered self-consistent when the energy change was smaller than 10^{-5} eV. A geometry optimization was considered convergent when the force change was smaller than 0.05 eV/Å. The Brillouin zone integral uses the surfaces structures of $2 \times 2 \times 1$ monkhorst pack K-point sampling (Pd (111) and Bi atom doped Pd (111)). Finally, the adsorption energies (E_{ads}) are calculated as E_{ads}= $E_{ad/sub}$ -E_{ad} -E_{sub}, where $E_{ad/sub}$, E_{ad} and E_{sub} are the optimized adsorbate/substrate system, the adsorbate in the structure and the clean substrate respectively. The U correction had been used for Pd atoms, which was set as 4.26 eV. The free energies are obtained by G=E_{total}+E_{ZPE}-TS, where E_{total}, E_{ZPE}, and TS are the ground-state energy, zero-point energies, and entropy terms, respectively, with the latter two taking vibration frequencies from DFT. Finally, the reaction energies (G) of different intermediates are defined as ΔG=G_i-$G_{reactant}$ (G_i is the energy of intermediates and $G_{reactant}$ is the total energy of reactants).

3. Results and discussions

3.1. Consideration factors of electrode materials

According to literature reports, currently the most-accepted mechanism for the selective oxidation of alcohols is a typical two-step oxidative dehydrogenation route: first, the oxidative addition of the O-H bond

species and the formation of alkoxide; then, α-hydrogen elimination from the alkoxide species to generate corresponding carbonyl compound. Palladium-based materials are typical electrocatalysts for alcohol oxidation, however, its electrocatalytic activity and selectivity are still far from being satisfactory. In these processes, the elimination of α-hydrogen from alkoxide species on palladium is the rate-controlling step in the alcohol oxidation [16–19]. The d-band center model proposed by Hammer and Nörskov has been widely and successfully used to elucidate and predict the catalytic activity of various electrocatalysts. In order to enhance the electrocatalytic activity and selectivity of Pd-based catalytic material, heterogenous metallic atoms of different atomic radius sizes can be introduced, producing metal alloy catalysts. Maximum current density (i_M) is used as criterion to evaluate the electro-oxidation performances of Pd based materials. Obviously, PdBi alloy grown on nickel foam (PdBi/NF) shows the highest 1, 3-P oxidation performances (Fig. S2a-c). The d-band center of these metals could also be obtained from XPS valence band spectra. According to the d-band center model proposed by Hammer and Nörskov, the high performance of PdBi/NF can be attributed to the proper d-band center, which implies the favorable adsorption energy of precursor organics on the catalyst surface Fig. S2d -l). Therefore, PdBi/NF is employed herein as the catalyst for further investigation.

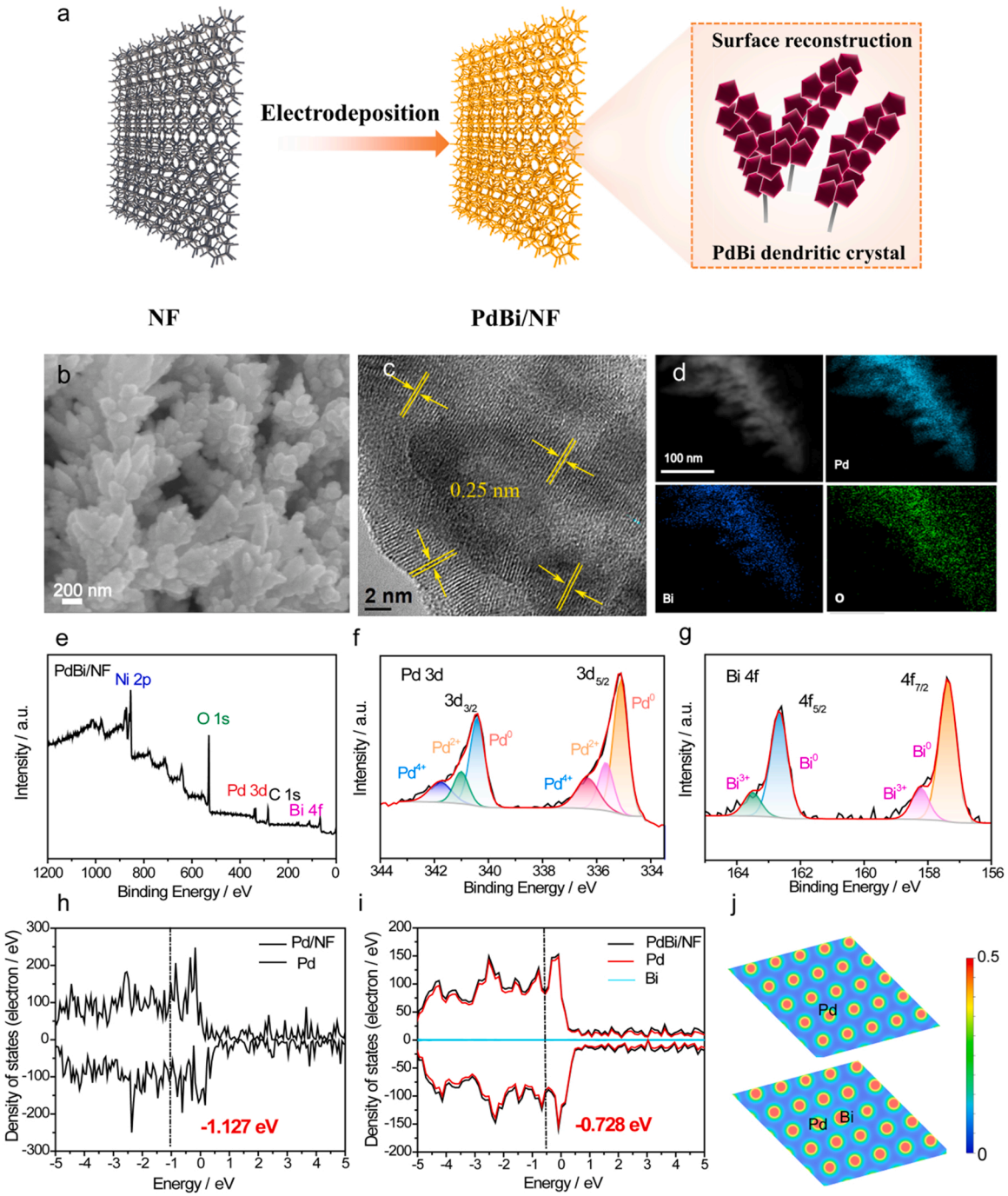

Fig. 2. Material Characterization of catalysts. (a) Schematic illustration of PdBi/NF syntheses. (b-g) Structural and morphological characterizations of PdBi/NF, (b) SEM image, (c) HR-TEM, (d) TEM-EDX mapping of PdBi/NF,(e) XPS survey spectrum of PdBi/NF, (f-g) High-resolution XPS spectra of Pd 3d, Bi 4 f of PdBi/NF, (h-i) Density of States of Pd (111) and Pd-Bi (111) surfaces from theoretical calculation, (j) Charge density distribution of Pd/NF and PdBi/NF.

3.2. Material Characterization and Performance

As illustrated in Fig. 2a, PdBi/NF has been synthesized by electrochemical deposition method at varied deposition time intervals and potentials, which shows a typical dendritic morphology.

Material characterization and performance of PdBi/NF and PdBi/NF-x (x = 1–5) have been investigated and the results are shown in Fig. S3-S6. The obtained PdBi/NF catalysts were firstly investigated by X-ray diffraction (XRD) and all these materials show similar XRD patterns as shown in Fig. S3. As shown in the local-enlarged XRD patterns of PdBi/NF (Fig. S3a), the obvious shift towards lower angles of the Pd (111) peaks of PdBi/NF can be found, which can be attributed to the lattice expansion induced by the incorporation of Bi atoms, implying the formation of the PdBi alloy [20,21]. The contribution of nickel foam to the anodic reaction is negligible (Fig. S4a) and the electrocatalytic performances of obtained PdBi/NF materials towards 1, 3-P were investigated (Fig. S4-S6). PdBi/NF synthesized at a constant potential of − 0.3 V vs SCE for 800 s shows the highest current density, lowest impedance and largest electrochemical surface area, therefore has been chosen for further studies (named PdBi/NF in the following text). Scanning electron microscopic (SEM, Fig. 2b), transmission electron microscopic (TEM, Fig. 2c) images, and X-ray photoelectron spectroscopic (XPS) spectra (Fig. 2e-g) also suggest the successful preparation of PdBi/NF. Lattice fringes of 0.25 nm in d-spacing can be clearly seen from the HRTEM image (Fig. 2c), corresponding to Pd (111) crystal facet though it is slightly larger than standard 0.224 nm, which can be attributed to the alloying of Bi atoms in Pd lattice, in consistence with XRD patterns. The lattice expansion and distortion would benefit the electrochemical catalytic performance enhancement of PdBi/NF [22–25]. The EDS results (Fig. 2d) indicate that PdBi/NF is composed of uniformly distributed Pd (91.64 wt%) and Bi (8.36 wt%) elements, while no other elements can be found. Fig. 2e-g proves that Pd, Bi elements mainly present in metallic forms in the PdBi/NF catalyst. Fig. 2h-i shows the density of states distributions of Pd/NF and PdBi/NF alloys by theoretical calculation. Clearly, upon doping Bi, the d orbital of Pd would be affected by coupling the p orbital and d orbital of Bi, therefore the density of states distribution of PdBi exhibits a relatively weak linearity and a continuous state, and the electrons of PdBi are within the energy level. The d-band center of the Pd changes from − 1.127 eV to − 0.728 eV which is close to the Fermi level favoring the adsorption of the organic molecule. Fig. 2j presents the charge density distributions for Pd/NF and PdBi/NF. After Bi doping, the charge distribution in the doped region is uniform, and the electron density of PdBi/NF is higher than that of Pd/NF, which makes the reaction thermodynamically more feasible.

The electrochemical measurements were performed in a 1.5 M KOH electrolyte containing 1 M 1, 3-P. All the potentials are referred to a reversible hydrogen electrode except for additional notes. Single-chamber electrolytic cells were used during liquid product detection, and H-type electrolytic cells were employed for hydrogen and O_2 production measurements to avoid crossover with cathode HER. The cyclic voltammetry (CV) curve in the blank electrolyte without the addition of 1 M 1, 3-P displays a strong peak centered at 1.39 V belonging to the oxidation of Ni (Fig. 3a). As a contrast, an appreciable current density enhancement can be found at 0.40 V after adding 1, 3-P, indicating the considerable electrocatalytic activity of PdBi/NF for 1, 3-P oxidation. Moreover, A current density of as high as 1300 mA cm^{-2} can be obtained for the selective oxidation of 1, 3-P due to the kinetically favorable 1, 3-P oxidation. In 2 h of electrocatalytic reaction, the product accumulated at the anode was confirmed to be 3-Hp according to the qualification results of ^{1}H and ^{13}C NMR spectroscopy (Fig. 3b, Fig. S7) and no other products were found. NMR results show that 1, 3-P has been selectively oxidized to 3-Hp: ^{1}H NMR (500 Hz, $(CD_3)_2S{=}O$, TMS), δ(ppm): 3.60 (t, 6.75 Hz, 2 H), 2.22 (t, 6.75 Hz, 2 H); ^{13}C NMR (125 Hz, $(CD_3)_2S{=}O$, TMS), δ(ppm): 180.02, 58.96, 40.27. Moreover, the yield of 3-Hp has also been measured in 2 h of reactions at varied applied potentials (Fig. 3c). In particular, the highest production of 5.2 mmol cm^{-2} h^{-1} of 3-Hp can be obtained at 1.0 − 1.1 V. At potentials more positive than 1.20 V, OER will take place and by product, 1, 3-malonic acid, will be generated and the production of 3-Hp become slowed down. Time-

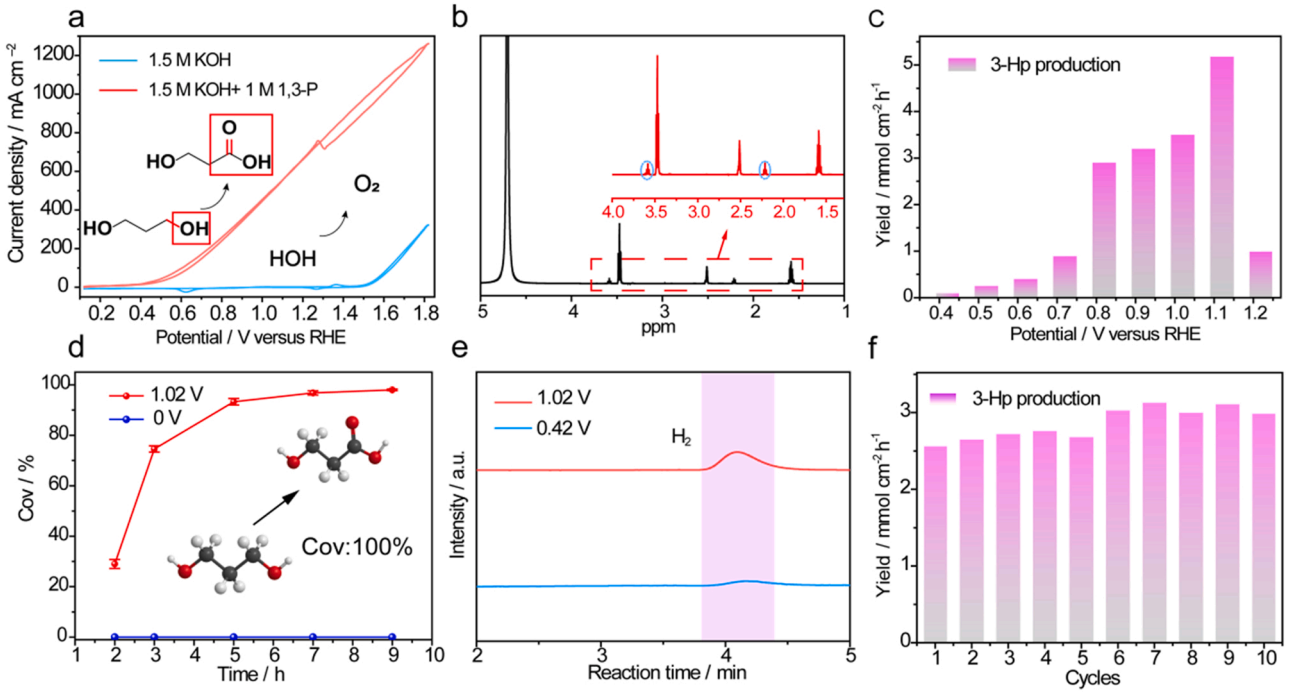

Fig. 3. 1, 3-P to 3-Hp oxidation using the PdBi/NF catalyst. (a) Cyclic voltammetric (CV) curves of PdBi/NF in 1.5 M KOH with or without the addition of 1, 3-P at a scan rate of 10 mV s^{-1}. (b) ^{1}H NMR spectra of 1, 3-P anodic oxidation products in 2 h of electrocatalytic reaction on PdBi/NF electrode. (c) Yield of PdBi/NF for 3-Hp by chronoamperometry for 2 h at varied voltages. (d) The conversion rate of 1, 3-P. (e) GC chromatograms of gaseous products for 1, 3-P oxidation (Argon as a carrier gas). (f) Cycle-dependent 3-Hp production at 1.02 V vs RHE.

dependent conversion at 1.02 V shows the complete electrooxidation of 1, 3-P in 48 h, and the conversion reaches above 95% in 7 h (Fig. 3d, Fig. S8). The control experiment without applied potential shows no production of 3-Hp after long-term test, excluding the self-oxidation of the reactant (Fig. 3d).

Excitingly, gaseous species was also produced at the anode, which was collected and analyzed. According to the gas chromatographic results, H_2 is the only anodic gas product from 1, 3-P oxidation over the PdBi/NF catalyst at the potentials lower than 1.42 V (Fig. S9a, Fig. 3e, Table. S1). The volume of H_2 gas produced from the 1, 3-P oxidation increases at prolonged electrolysis time periods (Fig. S9b) and has been measured to be 34.9 μL cm^{-2} h^{-1} at 1.02 V. Supporting electrochemical experiments have been carried out using H_2 and 3-Hp as the anode reactants to verify whether the PdBi/NF catalyst is active or not for these productions. As shown in Fig. S10, the PdBi/NF catalyst shows negligible activity towards H_2 and 3-Hp oxidation compared to that of 1, 3-P. Electrons source required for anodic hydrogen generation is a key issue but has always been ignored, which, herein, is assumed to originate from the oxidation of anode organics, namely, part of electrons released from the oxidation of the organics are used for the immediate in-situ anodic hydrogen evolution without entering the external circuit which will be discussed in detail in the next section of this manuscript.

According to the kinetics of alcohol oxidation, 1.02 V has been selected as the potential for the following in situ characterizations. Additionally, as shown in Fig. 3f, the stable and even slightly increased yield rate of 3-Hp at 1.02 V demonstrates the high durability of PdBi/NF. As plotted in Fig. S11, the cyclic voltammogram of PdBi/NF undergoing stability test at 1.02 V shows a higher current density than the initial PdBi/NF due to the activation of the catalyst which will be revealed by the following Raman spectroscopic results.

3.3. Two-electrode electrolysis performances

As illustrated in Fig. 4a, a two-electrode alkaline electrolyzer Pt ‖ PdBi/NF with or without membrane has been established for the co-electrolysis of water and 1, 3-P, which produces 3-Hp at the anode, and hydrogen at both cathode and anode, in contrast to the conventional HER system only producing H_2 at the cathode. In the electrolyzer without membrane, the hybrid electrolyzer coupling 1, 3-P oxidation (1, 3-POR) and HER only requires a 0.25 V cell voltage for generating 3-Hp and H_2, indicating much lowered energy consumption compared to conventional electrocatalytic water splitting (Fig. 4**b**). And to produce hydrogen at both anode and cathode, the electrolyze needs an applied voltage of as low as 0.86 V to achieve a current density of 20 mA cm^{-2} as shown in Fig. S12a. Moreover, as quantified by gas chromatography (GC), the hydrogen production rate is 18.49 μL cm^{-2} h^{-1} at the anode (Fig. S12b) and 3.21 mL cm^{-2} h^{-1} at the cathode (Fig. S12c) in H-type electrolytic cell equipped with membrane, and the total hydrogen production rate amount to 3.23 mL cm^{-2} h^{-1}. Meanwhile, a significantly higher 3-Hp production rate of 5.87 mg cm^{-2} h^{-1} has been obtained at the anode (Fig. S12b). Fig. S13 shows the standard curve of H_2 production measured by GC and the FE for cathodic hydrogen is 100% (Fig. 4c). What interested us is that the amount of charge required for hydrogen production at the cathode is significantly lower than that produced by the anodic alcohol oxidation. The electron transfer pathway is therefore reasoned to be distinctive from the previous literature reports. Peculiarly, it has also been found that the total charge consumed by the hydrogen productions at the anode and cathode is only slightly smaller than those generated from the oxidation of 1, 3-P (Fig. 4d) in this co-electrolysis system. Therefore, it is assumed that the electron donated by anodic alcohol oxidation is not only used for the cathodic HER through the circuit electron transfer, but also for the concurrent anodic hydrogen evolution without entering the circuit. The

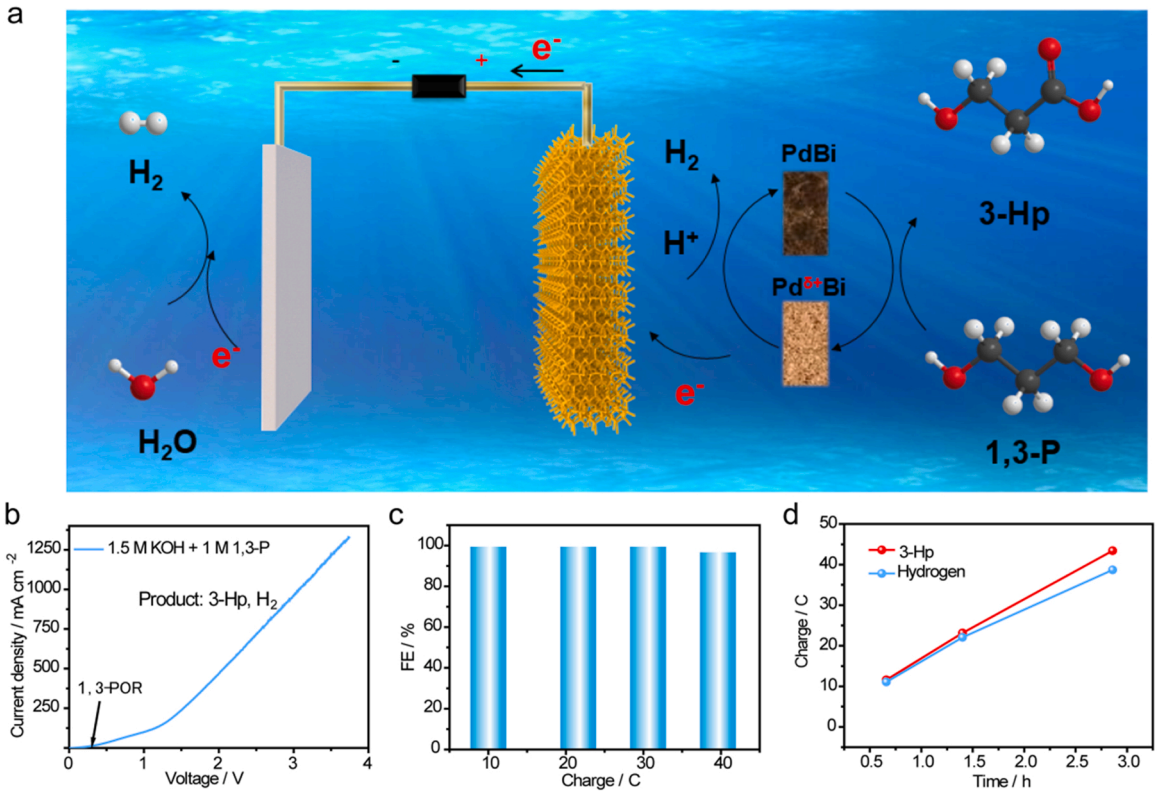

Fig. 4. Two-electrode electrolysis performances. (a) Scheme for the co-electrolysis of water and 1, 3-P. (b) LSV curves for the co-electrolysis of 1, 3-P and water in a two electrode system. (c) FE values for cathodic H_2 production at varied amount of transferred charges and (d) Charges consumed by anodic and cathodic hydrogen production and that generated by 1, 3-POR to 3-Hp in the two-electrode system tested at the cell voltage of 0.86 V.

small charge capacity difference between the donated ones from the anodic oxidation reaction and the consumed ones by HER at bipolar electrodes can also be well explained by following in-situ measurements.

3.4. Mechanism Study

The critical role of Bi in enhancing the electrocatalytic performance has been confirmed by XPS spectra. As shown in Fig. S14, high-resolution Pd 3d XPS spectra of PdBi/NF are significantly negative-shifted compared with that of Pd/NF, which indicates the electron enrichment at Pd atoms donated by Bi atoms. In the electrocatalytic conversion of 1, 3-P to 3-Hp, the preferred breakdown of the C-H bond with C-C bond being unaffected in the alkoxide species is critically important for the α-hydrogen atom deprivation. Here, negatively charged Pd is favorable for attacking C atom of C-H bond, forming a δ bond of Pd-C which strengthens the adsorption of alcohol organic molecules and donates electrons to C-H antibonding orbitals. Therefore, C-H bond can be activated by PdBi/NF while C-C bond remains relatively unaffected in the electrooxidation of 1, 3-P, and resultantly, the desired product, 3-Hp, can be obtained at favorably high activity and selectivity.

To have an insight into the mechanism of this reaction on PdBi/NF electrode, isotope labeling experiments were carried out to investigate the sources of hydrogen and oxygen elements in the produced 3-Hp. To

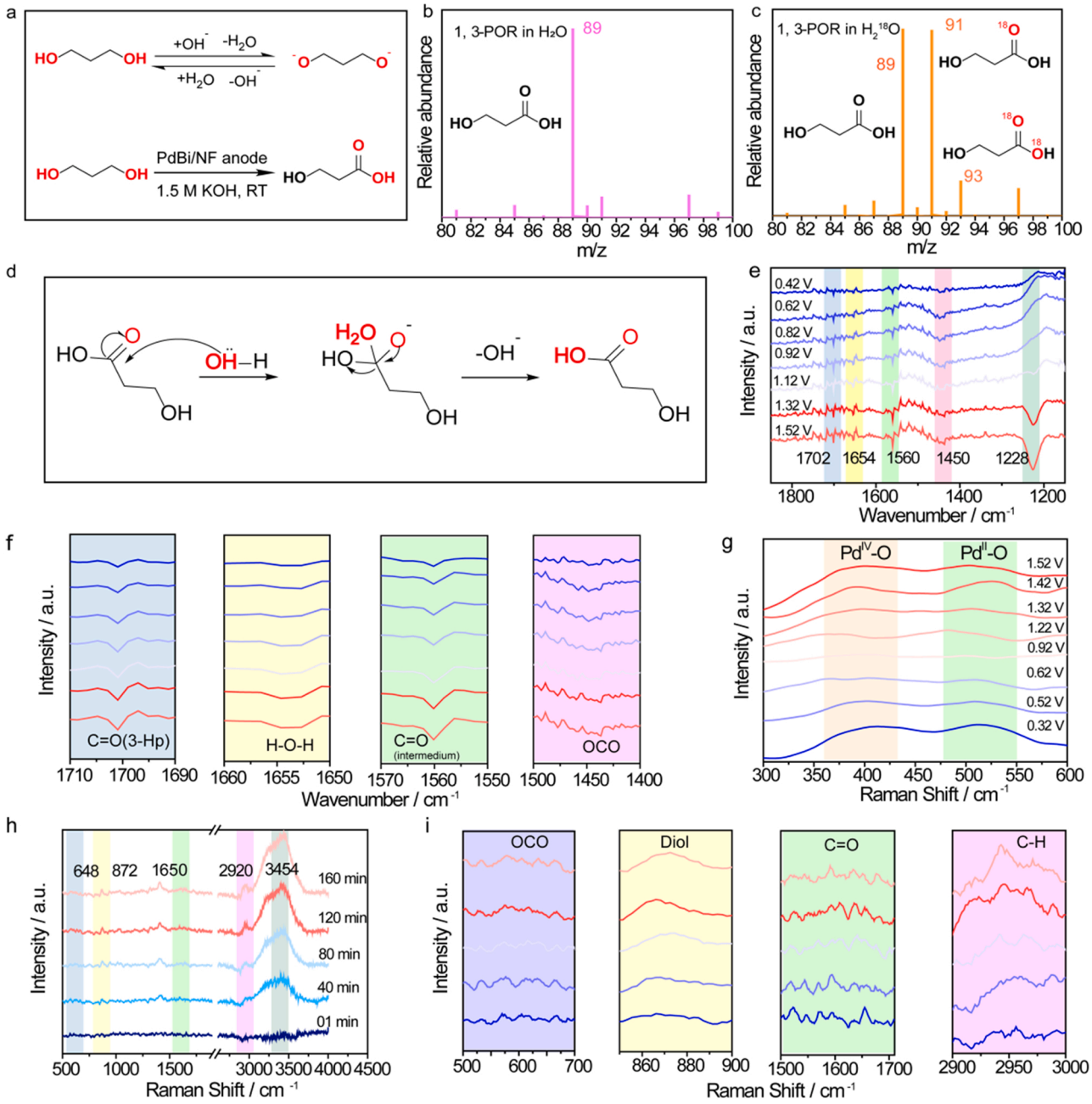

Fig. 5. Mechanism Study. (a) Acid-base equilibrium of 1, 3-P and 1, 3-POR to 3-Hp. (b-c) 1, 3-POR to 3-Hp in isotope labeled electrolyte. Mass spectra of 3-Hp ($m/z = 89$) obtained in H_2O solution (b) and 3-Hp ($m/z = 91/93$) in $H_2^{18}O$ solution (c). (d) Acid-base equilibrium and reaction of 3-Hp. (e-f) In situ Fourier transform infrared (FTIR) spectra of 1,3-P oxidation over PdBi/NF in 1.5 M KOH containing 1 M 1, 3-P electrolyte, and f displays the locally magnified details in e) at varied potentials. (g-i) In situ Raman spectra of the surface palladium species in PdBi/NF at varied potentials (g), and liquid product of 1, 3-P oxidation over PdBi/NF in 1.5 M KOH containing1 M 1,3-P electrolyte at varied periods at 1.02 V (h), and i shows the locally magnification in h.

this end, alkaline H_2O, D_2O, or $H_2^{18}O$ solutions (1.5 M KOH with 1 M 1, 3-P) were used for electrochemical 1, 3-P oxidation and the isotopomer distribution in the anodic product 3-Hp was analyzed by mass spectrometry (MS), either on a liquid chromatography (LC) or a gas chromatography (GC). The H atom in OH group of 1, 3-P can spontaneously exchange with water under the reaction conditions, suggesting the formation of alkoxide via the acid-base equilibrium (Fig. 5a). In D_2O solution, the *m/z* values of cathodic produced hydrogen are 2, 3, and 4, indicating that the hydrogen gas comes not only from deuterium but also from hydrogen atoms (Fig. S15). Simultaneously, the MS spectra of 3-Hp reveals that one ^{18}O atom in 3-Hp ($m/z = 91$) is originated from ^{18}O labeled water (Fig. 5b-c), suggesting that oxygen derived from water is involved in this reaction. The produced 3-Hp may undergo a nucleophilic substitution reaction with water, so a fraction of produced 3-Hp molecules have two oxygen atoms from water oxygen in each 3-Hp molecule featuring $m/z = 93$ (Fig. 5d) [26].

A series of quasi-in situ experiments were adopted to unveil the high-performance origination of 1, 3-P electrooxidation to 3-Hp and the reaction pathway during the anodic reaction in 1.5 M KOH over the PdBi/NF anode. Electrochemical in situ Fourier transform infrared (FTIR) spectroscopic detections were performed to trace bond rupture and formation during the reaction. Fig. 5e-f show spectral results of multi-step FTIR measurements on PdBi/NF electrode at varied potentials in 1.5 M KOH solution containing 1 M 1, 3-P. The downward interfacial water bands (δ(HOH) at $-1654\ cm^{-1}$) were detected on catalyst, indicating the adsorptions of OH and H_2O on the catalyst in this reaction. The intensity of 1560 cm^{-1} bands attributable to the ν(C═O) vibration of 3-hydroxypropanal becomes clearly higher at increased potentials, implying the bond rupture of C-H, which will be further oxidized to 3-hydroxypropionic acid. Meanwhile, the ν(CO) (1230–1225 cm^{-1}) region in Fig. 5e shifts to the longer wavelength at increased potentials, indicating the activation of hydroxyl group of 1, 3-P. The band at 1702 cm^{-1} belonging to C═O vibration in the carboxyl group significantly intensifies with the increase of potential, attributable to the formation of 3-hydroxypropionic acid (Fig. 5e). As the potential increases, the rather weak bands at 1450 and 1304 cm^{-1} respectively due to the asymmetric and symmetric stretching of ν(OCO) bands of interfacial 3-Hp species also become stronger. These results demonstrate that 1, 3-P is first dehydrogenated on surface sites, forming adsorbed 3-hydroxypropanal species, which may serve as an indispensable intermediate to be further oxidized to 3- Hp.

Electrochemical *operando* Raman spectroscopy is a powerful tool to investigate the structural evolution and active species of catalytic materials [27–29]. Firstly, potential-dependent *operando* Raman spectra show that the characteristic Raman band of Pd^{IV}-O (~ 400 cm^{-1}) and Pd^{II}-O (~ 530 cm^{-1}) emerge at 0.32 V vs RHE for PdBi/NF (Fig. 5 g) [30]. Probably, the super-surface metallic palladium atoms of PdBi/NF will be partially oxidized into Pd^{IV}-O and Pd^{II}-O by donating electrons to Pd-C and C-H bonds in the alkoxide, and the bonds break at the active site consequently. Notably, the Raman bands of Pd^{IV}-O and Pd^{II}-O become disappeared at the oxidation potentials in between 0.92 and 1.02 V vs RHE, suggesting the recovery of metallic palladium. At 0.92 and 1.02 V, the generated active hydrogen atoms will reduce the Pd^{IV}-O and Pd^{II}-O to metallic Pd [18]' [19,31,32]. With the further increase of the oxidation potential, the intensities of the two Raman bands increase again, which might be attributable to the Pd^0 to $Pd^{\delta+}$ conversion along with OER. These results demonstrate that the active species is metallic palladium for alcohol oxidation in PdBi/NF. The highest yield of 3-Hp can be obtained in the potential range of 0.92–1.02 V in correspondence with the breakage of the C-H bond in the alkoxide breaks, resulting in active hydrogen production accompanying the super-surface $Pd^{\delta+}$ reduction back into metallic Pd which lead to ultra-high activity and stability of catalyst [33,34]. This result indicates that a fraction of the electrons and α-H generated by 1, 3-P oxidation is used for catalyst reduction, which accounts for the electron deficiencies leading to the slightly lower electron consumption by bipolar hydrogen production than those generated by 1, 3-P oxidation. Time-dependent *operando* Raman spectra (Fig. S16) suggest that most surface Pd atoms are in an oxidized state at relatively low-potentials of around 0.4–0.5 V. Expectedly, the consumption rate of 1, 3-P is low, and the amount of electrons and α-H produced is insufficient at the low-potentials.

Furthermore, time-dependent *operando* Raman spectroscopy was employed to validate the adsorption mode of 1, 3-P on the PdBi/NF surface. Fig. 5h displays clearly the structural characteristic diol peaks of 1, 3-P (872 cm^{-1}), while the peak assigned to the C-H stretching vibration (2920 cm^{-1}) in CH_2 also demonstrates the adsorption of 1, 3-P on the PdBi/NF surface. The new peaks 1650 cm^{-1} assigned to the C═O stretching of 3-hydroxypropanal intensify in the time course at first, then reaches a plateau indicating the balanced formation and consumption of intermediates. As the time increases, the bands at 648 $cm^{-1}$and 3454 cm^{-1} due to the vibrations of OCO and -OH bonds of interfacial 3-Hp species emerges, suggesting the generation of 3-hydroxypropionic acid which are consistent with the FTIR results.

Pd/NF was also investigated by Raman spectroscopy under the reaction condition to explore the role of Bi in the 1, 3-P oxidation reaction. Potential-dependent *operando* Raman spectra (Fig. S17) shows the presence of characteristic bands of Pd^{IV}-O (400 cm^{-1}) and Pd^{II}-O (530 cm^{-1}) at the elevated potentials. Moreover, the band intensity keeps rapid increasing at the increased oxidation potential, and no further reduction of Pd can be found, indicating the deactivation of the catalyst. Time-dependent Raman spectra display two new peaks belonging to formic acid at 800–1100 cm^{-1}. The characteristic band of 3-Hp can be identified in twenty minutes of reaction for the product enrichment, which is significantly longer than PdBi/NF (Fig. S18), evidencing the breakage of C-C bonds and the slow kinetics of the reaction over Pd/NF [35]. Resultantly, Bi plays an indispensable role in enhancing the reaction activity, and more importantly, the selective formation of 3-hydroxypropionic acid product.

Density functional theory (DFT) calculation has also been used to investigate the reaction mechanism for the conversion from 1, 3- P to 3-Hp and H_2. The free energy changes during the reaction have been obtained when catalyzed by Pd and PdBi and the results are shown in Fig. 6a (calculation details can be found in the Methods section). From these calculations, the limiting step is the breakage of C-H bond in $*OHCH_2CH_2CHOOH$ intermediate (**V→VI**) due to its high free energy change of 1.08 eV and 0.83 eV catalyzed by Pd and PdBi, respectively, demonstrating enhanced kinetics upon bismuth doping.

Based on the XPS, FTIR and Raman results and discussions above, a reaction mechanism can be proposed for the efficient electrochemical conversion of 1, 3-P to 3-Hp catalyzed by PdBi/NF. Firstly, the introduced Bi in the Pd lattice donate electrons to Pd, resulting in negatively charged palladium atoms, which benefits the 1, 3-P adsorption on PdBi/NF catalyst and the strengthening of palladium-carbon (Pd-C) bonds (**II**) [36]. Next the enriched electrons around Pd can be withdrawn much stronger by the adsorbed 1, 3-P molecules, leading to the palladium oxidation into Pd^{IV}-O and Pd^{II}-O and the electron filling in the C-H antibonding orbital, and the consequent C-H bond breakage. As shown in Fig. 6b, the alcohol molecule initially undergoes H_α deprotonation into more active alkoxide via base catalysis(**III**) [37,38], which is then oxidized by the nucleophilic OH^- on the surface of PdBi /NF for α-H elimination to corresponding 3-hydroxypropanal (**IV→V**). A part of the α-H atoms participate in the reduction of the oxidized Pd back into metallic palladium (**ii in** Fig. 6c), while the other part of α-H atoms bond with each other to produce hydrogen (**i in** Fig. 6c) gas via Tafel recombination (**V→VI**) or combine with OH^- for water generation. The following nucleophilic attack by OH^- onto electrophilic carbocation in hydroxypropanal generates negatively charged hydroxycarboxylic acid, which, subsequently, is converted to hydroxycarboxylic acid product on the electrocatalyst (**VI**). All the electrons for electrocatalyst regeneration, anode and cathode hydrogen production come from anode organic oxidation. Overall, the H and e transfer pathways have been revealed. Fractions of hydrogen atoms and electrons from the oxidation of the

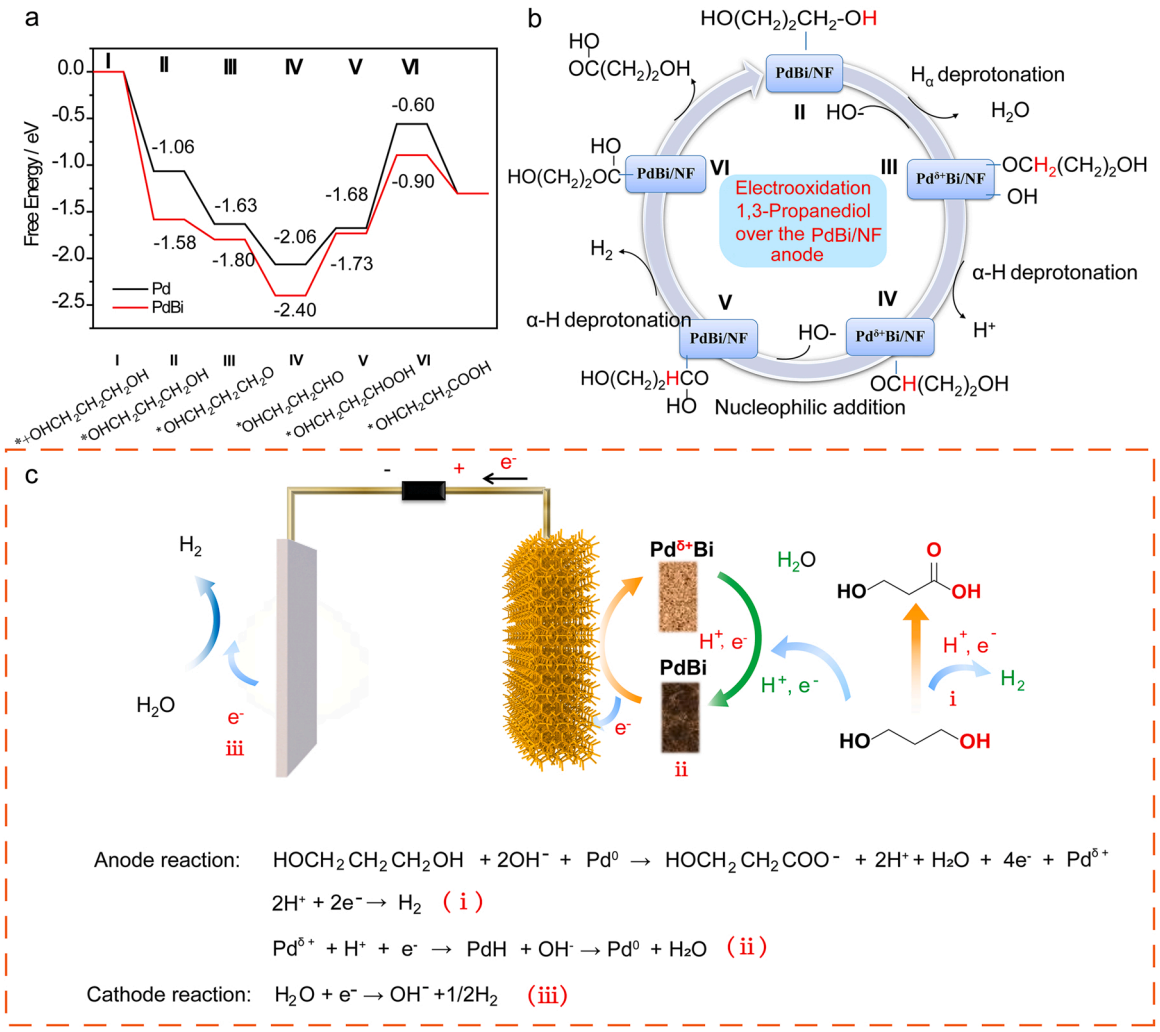

Fig. 6. Density functional theory calculations for 1, 3-P to 3-Hp and reaction mechanism. (a) Free energy diagrams for the oxidation of 1, 3-P to 3-Hp, (b) A plausible tandem oxidation reaction mechanism for electrochemical 1, 3-P oxidation, (c) The proposed electron and α-H transfer pathways for the present co-electrolysis system. The green represents electron and α-H donation (alcohol oxidation to corresponding carboxylic acid) while the red represents electron and α-H consumption (i: anodic HER; ii: catalyst activation; iii: cathodic HER).

alcohol are used distinctively for the hydrogen production and electrocatalyst regeneration at the anode (**i and ii in** Fig. 6c), in the meantime, the remaining electrons will transfer through the external circuit for cathodic hydrogen production (**iii in** Fig. 6c).

3.5. The Methodology Generality

The application generality of PdBi/NF towards the oxidation of α-H armed alcohols for concurrent productions of value-added chemicals and hydrogen at anode is examined (Fig. 7, Fig. S19-20). A series of alcohol molecules armed with α-H can be converted to the corresponding α-H-deprotonated products and hydrogen with high conversions and selectivity under the same reaction conditions. For example, 1, 4-butanediol and 1, 5-pentanediol can be electro-oxidatively converted to 4-hydroxybutyric acid and 5-hydroxy-valeric acid, respectively. Both n-propanol and isopropanol can be oxidized into the corresponding ketone products by α-H deprivation. Glycerol and 1, 2-Propanediol can be deprotonated of α-H into hydroxycarboxylic acid.

4. Conclusions

A co-production system for both hydrogen from bipolar electrodes and value-added chemicals at anode has been established by the co-electrocatalysis of water and α-H-armed alcohol molecules. In particular, both 3-Hp and hydrogen can be concurrently obtained at the anode, which is accompanied by efficient HER at the cathode. More importantly, the unusual hydrogen and electron transfer pathways have been revealed. Fractions of hydrogen atoms and electrons from the oxidation of the alcohol are used distinctively for hydrogen production and electrocatalyst regeneration at the anode, which has been mostly overlooked in previous reports. Simultaneously, the remaining fraction of the electrons transfer through the circuit for cathodic hydrogen production. In brief, the adsorbed alcohol molecules convert to corresponding hydroxypropanal by deprotonating their α-H atoms, and a part of deprived α-H is consumed in reducing the oxidized Pd in the above reaction back into metallic palladium, while the other part of deprived H atoms are converted to hydrogen gas via Tafel recombination or H_2O. Then the nucleophilic attack by OH^- onto electrophilic carbocation in hydroxypropanal produces the final hydroxycarboxylic acid product. Substantially high 3-Hp and bipolar H_2 production rates of 5.87 mg cm^{-2} h^{-1} and 3.23 mL cm^{-2} h^{-1} were obtained, respectively. The present study heralds a new and promising method for the regulations of electron and α-H pathways for the enhanced atom and electron economy.

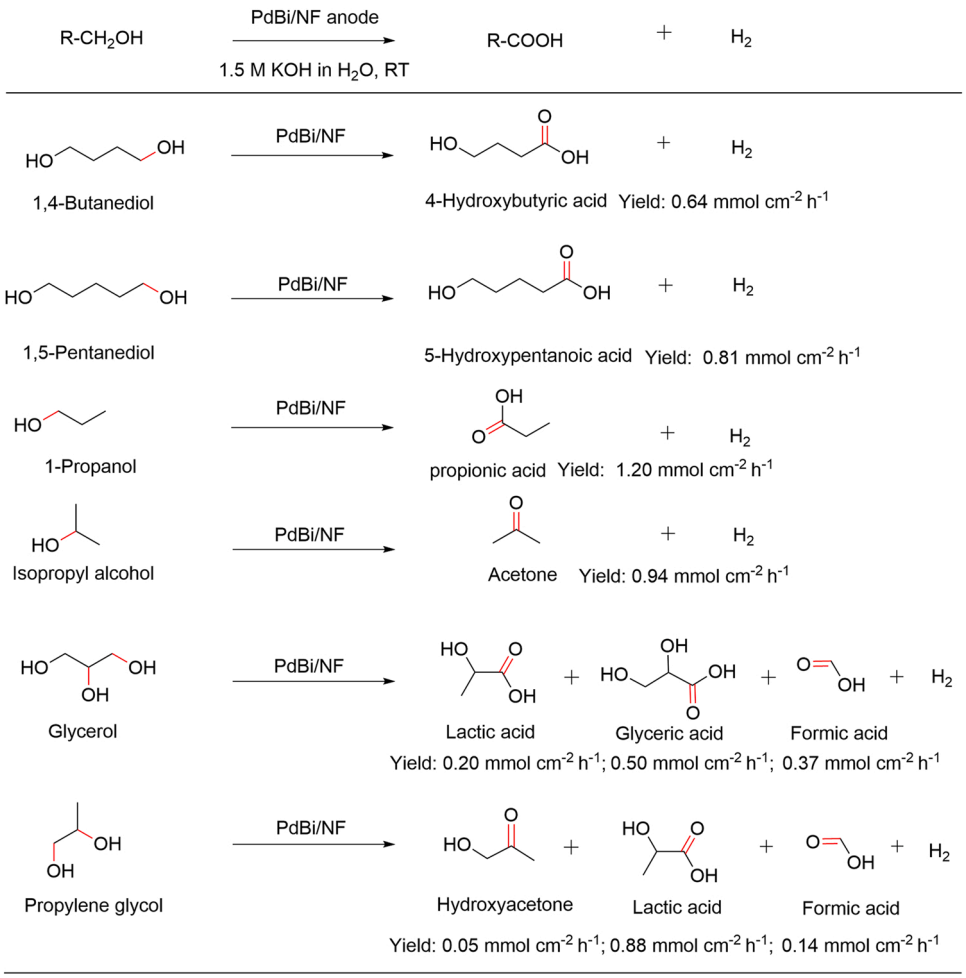

Fig. 7. Selective electro-oxidation reactions of a series of α-H-armed alcohol molecules.

CRediT authorship contribution statement

Di Si: Sample preparation, Electrochemical testing, Data analysis and sorting, Writing manuscript. **Min Wang**: Data analysis. **Xue Yang**: Data sorting. **Cheng Wang**: Data sorting. **Kai Shi**: Data sorting. **Bingji Huang**: Image analysis. **Lisong Chen**: Revision of manuscript, Validation, Funding acquisition. **Jianlin Shi**: Revision of manuscript, Validation, Funding acquisition.

Declaration of Competing Interest

The authors declare that they have no known competing financial interests or personal relationships that could have appeared to influence the work reported in this paper.

Acknowledgements

This work was supported by SINOPEC Research Institute of Petroleum Processing, National Key Research and Development Program of China (2022YFB4002700), Shanghai Science and Technology Committee Rising-Star Program (22QA1403400) and the Natural Science Foundation of Shanghai (21ZR1418700). The authors would like to thank ECNU Multifunctional Platform for Innovation for support of SEM and TEM characterizations (004).

Author Contribution

All authors have given approval to the final version of the manuscript.

Appendix A. Supporting information

Supplementary data associated with this article can be found in the online version at doi:10.1016/j.apcatb.2023.122664.

References

[1] S. Chu, A. Majumdar, Opportunities and challenges for a sustainable energy future, Nature 488 (2012) 294–303, https://doi.org/10.1002/fes3.229.
[2] L. Lin, W. Zhou, R. Gao, S. Yao, X. Zhang, W. Xu, S. Zheng, Z. Jiang, Q. Yu, Y. Li, C. Shi, X. Wen, D. Ma, Low-temperature hydrogen production from water and methanol using Pt/α-MoC catalysts, Nature 544 (2017) 80–83, https://doi.org/10.1038/nature21672.
[3] H. Li, C. Tsai, A. Koh, L. Cai, A. Contryman, A. Fragapane, J. Zhao, H. Han, H. Manoharan, F. Pedersen, J. Nørskov, X. Zheng, Activating and optimizing MoS2 basal planes for hydrogen evolution through the formation of strained sulphur vacancies, Nat. Mater. 15 (2016) 48–53, https://doi.org/10.1038/nmat4564.
[4] C. Kuai, Z. Xu, C. Xi, A. Hu, Z. Yang, Y. Zhang, C. Sun, L. Li, D. Sokaras, C. Dong, S. Qiao, X. Du, F. Lin, Phase segregation reversibility in mixed-metal hydroxide water oxidation catalysts, Nat. Catal. 3 (2020) 743–753, https://doi.org/10.1038/s41929-020-0496-z.
[5] K. Gong, F. Du, Z. Xia, M. Durstock, L. Dai, Nitrogen-doped carbon nanotube arrays with high electrocatalytic activity for oxygen reduction, Science 323 (2009) 760–764, https://doi.org/10.1126/science.1168049.
[6] (a) F.J.S.E. Barbir, PEM electrolysis for production of hydrogen from renewable energy sources, Sol. Energy 78 (2005) 661–669, https://doi.org/10.1016/j.solener.2004.09.003;
(b) Y. Zhong, et al., Recent progress in electrochemical C–N coupling reactions, 2667-1417, eScience (2022), https://doi.org/10.1016/j.esci.2022.11.002;
(c) L. Chen, J. Shi, Co-electrolysis toward value-added chemicals, Sci. China Mater. 65 (2022) 1–9, https://doi.org/10.1007/s40843-021-1809-5;
(d) Y. Li, X. Wei, L. Chen, J. Shi, M. He, Nickel-molybdenum nitride nanoplate

electrocatalysts for concurrent electrolytic hydrogen and formate productions, Nat. Commun. 10 (2019) 5335, https://doi.org/10.1038/s41467-019-13375-z.
[7] (a) T. Wang, L. Tao, X. Zhu, C. Chen, W. Chen, S. Du, Y. Zhou, B. Zhou, D. Wang, C. Xie, P. Long, W. Li, Y. Wang, R. Chen, Y. Zou, X.-Z. Fu, Y. Li, X. Duan, S. Wang, Combined anodic and cathodic hydrogen production from aldehyde oxidation and hydrogen evolution reaction, Nat. Catal. 5 (2022) 66–73, https://doi.org/10.1038/s41929-021-00721-y;
(b) H. Liu, N. Agrawal, A. Ganguly, Y. Chen, J. Lee, J. Yu, W. Huang, M. Mark, M. Janik, W. Li, Ultra-low voltage bipolar hydrogen production from biomass-derived aldehydes and water in membrane-less electrolyzers, Energy Environ. Sci. 15 (2022) 4175–4189, https://doi.org/10.1039/D2EE01427K.
[8] R.K. Saxena, P. Anand, S. Saran, J.J.B. a Isar, Microbial production of 1,3-propanediol: recent developments and emerging opportunities, Biotechnol. Adv. 27 (2009) 895–913, https://doi.org/10.1016/j.biotechadv.2009.07.003.
[9] V. Kumar, S. Ashok, S. Park, Recent advances in biological production of 3-hydroxypropionic acid, Biotechnol. Adv. 31 (2013) 945–961, https://doi.org/10.1016/j.biotechadv.2013.02.008.
[10] K.R. Kildegaard, N.B. Ensen, K. Schneider, E. Czarnotta, E. Oezdemir, T. Klein, J. Maury, B.E. Ebert, H.B. Christensen, Y. Chen, I.-K. Kim, M.J. Herrgard, L. M. Blank, J. Forster, J. Nielsen, I. Borodina, Engineering and systems-level analysis of Saccharomyces cerevisiae for production of 3-hydroxypropionic acid via malonyl-CoA reductase-dependent pathway, Microb. Cell. Fact. 15 (2016) 53, https://doi.org/10.1186/s12934-016-0451-5.
[11] S.M. Raj, C. Rathnasingh, J.-E. Jo, S. Park, Production of 3-hydroxypropionic acid from glycerol by a novel recombinant Escherichia coli BL21 strain, Process. Biochem. 43 (2008) 1440–1446, https://doi.org/10.1016/j.procbio.2008.04.027.
[12] C. Rathnasingh, S.M. Raj, J.-E. Jo, S. Park, Development and evaluation of efficient recombinant escherichia coli strains for the production of 3-hydroxypropionic acid from glycerol, Biotechnol. Bioeng. 104 (2009) 729–739, https://doi.org/10.1002/bit.22429.
[13] F. de Fouchecour, A.-K. Sanchez-Castaneda, C. Saulou-Berion, H.E. Spinnler, Process engineering for microbial production of 3-hydroxypropionic acid, Biotechnol. Adv. 36 (2018) 1207–1222, https://doi.org/10.1016/j.biotechadv.2018.03.020.
[14] X. Jiang, X. Meng, M. Xian, Biosynthetic pathways for 3-hydroxypropionic acid production, Appl. Microbiol. Biotechnol. 82 (2009) 995–1003, https://doi.org/10.1007/s00253-009-1898-7.
[15] B. Hu, M. Prashad, D. Har, K. Prasad, O. Repic, T.J. Blacklock, An efficient synthesis of (R)-2-butyl-3-hydroxypropionic acid, Org. Process Res Dev. 11 (2007) 90–93, https://doi.org/10.1021/op060199l.
[16] D. Si, B. Xiong, L. Chen, J. Shi, Highly selective and efficient electrocatalytic synthesis of glycolic acid in coupling with hydrogen evolution, Chem. Catal. 1 (2021) 941–955, https://doi.org/10.1016/j.checat.2021.08.001.
[17] T. Mallat, A. Baiker, Oxidation of alcohols with molecular oxygen on solid catalysts, Chem. Rev. 104 (2004) 3037–3058, https://doi.org/10.1021/cr0200116.
[18] R. DiCosimo, G.M. Whitesides, Oxidation of 2-propanol to acetone by dioxygen on a platinized electrode under open-circuit conditions, J. Phys. Chem. 93 (1989) 768–775, https://doi.org/10.1021/j100339a051.
[19] P. Vinke, H. Dam, H.V. Bekkum, Platinum catalyzed oxidation of 5-hydroxymethylfurfural, Stud. Surf. Sci. Catal. 55 (1990) 147–158, https://doi.org/10.1016/S0167-2991(08)60144-5.
[20] H. Xu, K. Zhang, B. Yan, J. Wang, C. Wang, S. Li, Z. Gu, Y. Du, P. Yang, Ultra-uniform PdBi nanodots with high activity towards formic acid oxidation, J. Power Sources 356 (2017) 27–35, https://doi.org/10.1016/j.jpowsour.2017.04.070.
[21] D. Bin, B. Yang, F. Ren, K. Zhang, P. Yang, Y. Du, Facile synthesis of PdNi nanowire networks supported on reduced graphene oxide with enhanced catalytic performance for formic acid oxidation, J. Mater. Chem. A 3 (2015) 14001–14006, https://doi.org/10.1039/C5TA02829A.
[22] W. Jiao, C. Chen, W. You, X. Zhao, J. Zhang, Y. Feng, P. Wang, R. Che, Hollow palladium-gold nanochains with periodic concave structures as superior ORR electrocatalysts and highly efficient SERS substrates, Adv. Energy Mater. 10 (2020) 1904072, https://doi.org/10.1002/aenm.201904072.
[23] Y. Feng, Q. Shao, Y. Ji, X. Cui, Y. Li, X. Zhu, X. Huang, Surface-modulated palladium-nickel icosahedra as high-performance non-platinum oxygen reduction electrocatalysts, Sci. Adv. 4 (2018) 8817, https://doi.org/10.1126/sciadv.aap8817.
[24] Z. Xia, S. Guo, Strain engineering of metal-based nanomaterials for energy electrocatalysis, Chem. Soc. Rev. 48 (2019) 3265–3278, https://doi.org/10.1039/C8CS00846A.
[25] S. Sarkar, U. Subbarao, S.C. Peter, Evolution of dealloyed $PdBi_2$ nanoparticles as electrocatalysts with enhanced activity and remarkable durability in hydrogen evolution reactions, J. Mater. Chem. A 5 (2017) 15950–15960, https://doi.org/10.1039/C7TA03673F.
[26] H. Zhou, Z. Li, S.-M. Xu, L. Lu, M. Xu, K. Ji, R. Ge, Y. Yan, L. Ma, X. Kong, L. Zheng, H. Duan, Selectively upgrading lignin derivatives to carboxylates through electrochemical oxidative C(OH)-C bond cleavage by a Mn-doped cobalt oxyhydroxide catalyst, Angew. Chem. Int. Ed. 60 (2021) 8976–8982, https://doi.org/10.1002/anie.202015431.
[27] Y. Huang, X. Chong, C. Liu, Y. Liang, B. Zhang, Boosting hydrogen production by anodic oxidation of primary amines over a NiSe nanorod electrode, Angew. Chem. Int. Ed. 57 (2018) 13163–13166, https://doi.org/10.1002/anie.201807717.
[28] J.-C. Dong, X.-G. Zhang, V. Briega-Martos, X. Jin, J. Yang, S. Chen, Z.-L. Yang, D.-Y. Wu, J.M. Feliu, C.T. Williams, Z.-Q. Tian, J.-F. Li, In situ Raman spectroscopic evidence for oxygen reduction reaction intermediates at platinum single-crystal surfaces, Nat. Energy 4 (2019) 60–67, https://doi.org/10.1038/s41560-018-0292-z.
[29] Y.-H. Wang, J.-B. Le, W.-Q. Li, J. Wei, P.M. Radjenovic, H. Zhang, X.-S. Zhou, J. Cheng, Z.-Q. Tian, J.-F. Li, In situ spectroscopic insight into the origin of the enhanced performance of bimetallic nanocatalysts towards the oxygen reduction reaction (ORR), Angew. Chem. Int. Ed. 58 (2019) 16062–16066, https://doi.org/10.1002/anie.201908907.
[30] A. Gannouni, X. Rozanska, B. Albela, M.S. Zina, F. Delbecq, L. Bonneviot, A. Ghorbel, Theoretical and experimental investigations on site occupancy for palladium oxidation states in mesoporous Al-MCM-41 materials, J. Catal. 289 (2012) 227–237, https://doi.org/10.1016/j.jcat.2012.02.014.
[31] G. Lin, Q. Ju, X. Guo, W. Zhao, S. Adimi, J. Ye, Q. Bi, J. Wang, M. Yang, F. Huang, Intrinsic electron localization of metastable MoS_2 boosts electrocatalytic nitrogen reduction to ammonia, Adv. Mater. 33 (2021) 2007509, https://doi.org/10.1002/adma.202007509.
[32] H.E. Vandam, L.J. Wisse, H.J.A.C. Vanbekkum, Platinum/carbon oxidation catalystsVIII. Selecting a metal for liquid-phase alcohol oxidations, Appl. Catal. 61 (1990) 187–197, https://doi.org/10.1016/S0166-9834(00)82143-0.
[33] S. Han, C. Wang, Y. Wang, Y. Yu, B. Zhang, Electrosynthesis of Nitrate via the Oxidation of Nitrogen on Tensile-Strained Palladium Porous Nanosheets, Angew. Chem. Int. Ed. 60 (2021) 4474–4478, https://doi.org/10.1002/anie.202014017.
[34] H. Wang, B. Jiang, T.-T. Zhao, K. Jiang, Y.-Y. Yang, J. Zhang, Z. Xie, W.-B. Cai, Electrocatalysis of ethylene glycol oxidation on bare and bi modified Pd concave nanocubes in alkaline solution: an interfacial infrared spectroscopic investigation, Acs. Catal. 7 (2017) 2033–2041, https://doi.org/10.1021/acscatal.6b03108.
[35] C. Liu, R. Li, W. Zhou, Y. Liang, Y. Shi, R.-L. Li, Y. Ling, Y. Yu, J. Li, B. Zhang, Selectivity origin of organic electrosynthesis controlled by electrode materials: a case study on pinacols, Acs. Catal. 11 (2021) 8958–8967, https://doi.org/10.1021/acscatal.1c01382.
[36] A. Winiwarter, L. Silvioli, S.B. Scott, K. Enemark-Rasmussen, M. Saric, D. B. Trimarco, P.C.K. Vesborg, P.G. Moses, I.E.L. Stephens, B. Seger, J. Rossmeisl, I. Chorkendorff, Towards an atomistic understanding of electrocatalytic partial hydrocarbon oxidation: propene on palladium, Energy Environ. Sci. 12 (2019) 1055–1067, https://doi.org/10.1039/C8EE03426E.
[37] Y. Kwon, S. Lai, P. Rodriguez, M. Koper, Electrocatalytic oxidation of alcohols on gold in alkaline media: base or gold catalysis, ? J. Am. Chem. Soc. 133 (2011) 6914–6917, https://doi.org/10.1021/ja200976j.
[38] H. Tao, Y. Xu, X. Huang, J. Chen, L. Pei, J. Zhang, J. Chen, B. Liu, A general method to probe oxygen evolution intermediates at operating conditions, Joule 3 (2019) 1498–1509, https://doi.org/10.1016/j.joule.2019.03.012.